nature astronomy

Article

https://doi.org/10.1038/s41550-023-02035-4

Evidence for baryon acoustic oscillations from galaxy–ellipticity correlations

Received: 18 July 2022

Accepted: 14 June 2023

Published online: 27 July 2023

Check for updates

Kun Xu [1,2], Y. P. Jing [1,3] ✉, Gong-Bo Zhao [4,5,6] & Antonio J. Cuesta [7]

The baryon acoustic oscillation feature in the clustering of galaxies or quasars provides a 'standard ruler' for distance measurements in cosmology. In this work, we report a 2–3σ signal of the baryon acoustic oscillation dip feature in the galaxy density–ellipticity cross-correlation functions using the spectroscopic sample of the Baryon Oscillation Spectroscopic Survey CMASS, combined with the deep Dark Energy Spectroscopic Instrument Legacy Imaging Surveys for precise galaxy shape measurements. We measure the galaxy–ellipticity correlation functions and model them using the linear alignment model. We constrain the distance D_V/r_d to redshift 0.57 to a precision of 3–5%, depending on the details of modelling. The galaxy–ellipticity measurement reduces the uncertainty of distance measurement by ~10% on top of that derived from the galaxy–galaxy correlation. More importantly, for future large and deep galaxy surveys, the independent galaxy–ellipticity measurements can help sort out the systematics in the baryon acoustic oscillation studies.

Measuring the expansion history of the Universe is one of the key goals in cosmology. The best constraints now are those from the measurements of the distance–redshift relation over a wide range of redshifts[1]. The baryon acoustic oscillation (BAO) feature in the clustering of galaxies is a standard ruler for robust distance measurements[2,3]. BAOs arise from tight coupling of photons and baryons in the early Universe. Sound waves travel through this medium and give rise to a characteristic scale in the density perturbations, corresponding to the propagation distance of the waves before the recombination. With large galaxy surveys, using BAOs, distances have been measured to a per cent level at various redshifts[4–8].

In the aforementioned studies, only the spatial distributions of galaxies are used, and the shapes and orientations of galaxies are ignored. The intrinsic alignment (IA) of galaxies is usually treated as a contaminant in weak-lensing analysis[9,10]. However, as we will demonstrate using actual observations in this work, IA is actually a promising cosmological probe and contains valuable information. The galaxy–ellipticity (GI) and ellipticity–ellipticity (II) IAs were first detected in luminous red galaxies[11,12,13]. Studies showed that the IA of galaxies can be related to the gravitational tidal field using the linear alignment (LA) model[14–16]. According to the LA model, a BAO feature in both GI and II correlations shows up as a dip, rather than a peak[17,18,19] as seen in the galaxy–galaxy (GG) correlations. Furthermore, the entire two-dimensional and anisotropic pattern of GI and II correlations may provide information additional to that of the BAOs. The results were tested and confirmed in N-body simulations[20]. Taruya and Okumura[21] also performed a forecast of cosmological constraints for IA statistics using the LA model, and found that IA can provide a similar level of constraints on cosmological parameters to the galaxy spatial distributions.

In this Article, we report a measurement of the BAO feature using IA statistics, namely GI, and confirm that IA can provide additional information to GG correlations. In addition to reducing statistical uncertainties of the distance measurements, GI can also provide a test of systematics when compared with the BAO measurements from GG. Details of this analysis, including the datasets, measurements

[1]Department of Astronomy, School of Physics and Astronomy, Shanghai Jiao Tong University, Shanghai, People's Republic of China. [2]Institute for Computational Cosmology, Durham University, Durham, UK. [3]Tsung-Dao Lee Institute and Shanghai Key Laboratory for Particle Physics and Cosmology, Shanghai Jiao Tong University, Shanghai, People's Republic of China. [4]National Astronomy Observatories, Chinese Academy of Sciences, Beijing, People's Republic of China. [5]University of Chinese Academy of Sciences, Beijing, People's Republic of China. [6]Institute for Frontiers in Astronomy and Astrophysics, Beijing Normal University, Beijing, People's Republic of China. [7]Departamento de Física, Universidad de Córdoba, Córdoba, Spain. ✉e-mail: ypjing@sjtu.edu.cn

https://doi.org/10.1038/s41550-023-02035-4

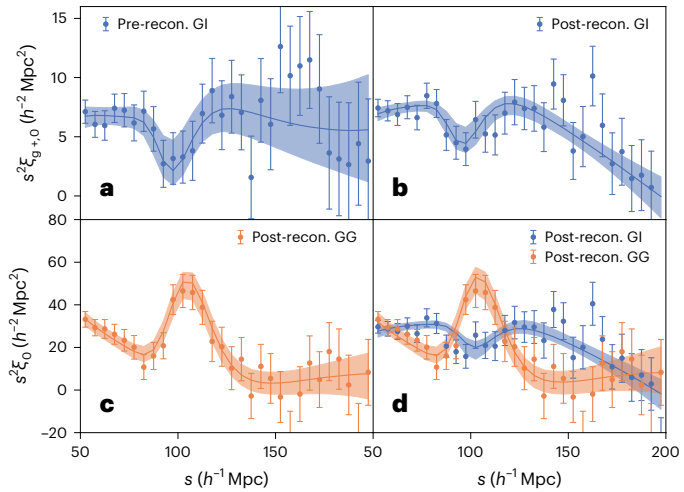

Fig. 1 | Measurements and modelling of GI and GG correlation functions. **a**, Pre-reconstruction GI correlations. **b**, Post-reconstruction GI correlations. **c**, Post-reconstruction GG correlations. **d**, Post-reconstruction combined modelling (GI multiplied by 4 for better illustration). Points and error bars show the mean and s.e.m. of clustering measurements. Errors are from the diagonal elements of the jackknife covariance matrices estimated using 400 subsamples. Lines and shading are the best-fit models and 68% confidence-level regions derived from the marginalized posterior distributions.

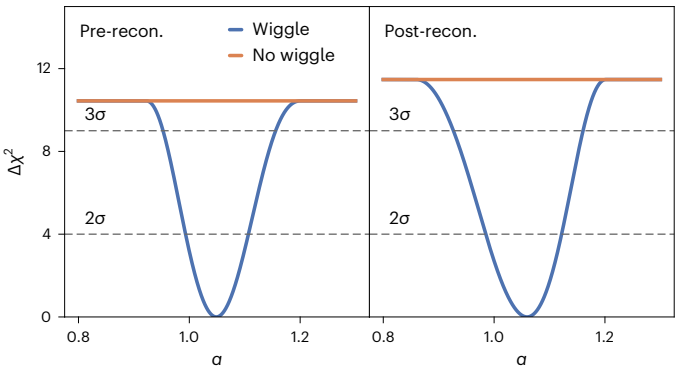

Fig. 2 | Plot of $\Delta\chi^2$ versus α for the pre- (left) and post- (right) reconstruction GI correlations. Orange lines show the $\Delta\chi^2$ for non-BAO models and blue lines those for BAO models.

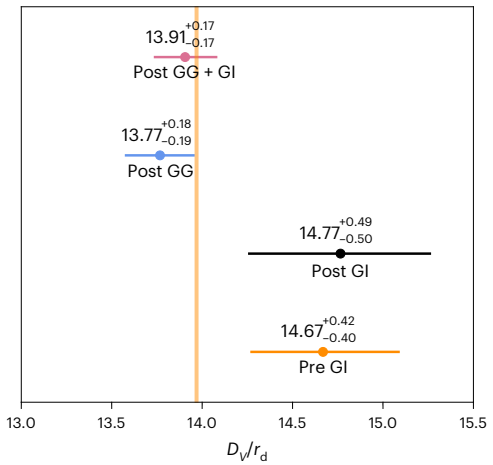

Fig. 3 | Constraints of D_V/r_d from GG and GI correlation functions with N_{JK} = 400. A combined post-reconstructed GG + GI constraint is also provided. The central values are the medians, and the error bars are the 16th and 84th percentiles. The vertical orange line shows the fiducial Planck18 results.

and modelling, are presented in Methods. Our fiducial results, as shown in the main text, are derived using data vectors in the range of 50–200 h^{-1} Mpc with a polynomial marginalized over. This range is chosen to ensure that the polynomial captures the entire shape and to avoid the turnover around 20 h^{-1} Mpc. For completeness, we also show results with other choices of the fitting range and with or without marginalizing over the polynomial in Supplementary Figs. 4 and 5 and Supplementary Table 1. We observe a 2–3σ BAO signal in all of these variations.

The measurements and modelling of the isotropic GI and GG correlation functions are shown in Fig. 1. The GI measurements show an apparent dip around the BAO scale at ~100 h^{-1} Mpc from both the pre- (panel a) and post-reconstructed samples (panel b). The fitting results are reasonable on all scales, namely, the reduced χ^2 is 0.97 for pre-reconstruction and 0.87 for post-reconstruction. To show the significance of the BAO detection, we display the $\Delta\chi^2 \equiv \chi^2 - {\chi_{\rm min}}^2$ surfaces in Fig. 2 (see also Supplementary Fig. 1), where ${\chi_{\rm min}}^2$ is the χ^2 for the best-fitting model. We compare $\Delta\chi^2$ for the no-wiggle model with the BAO model and find a 3σ detection of the BAO feature in both the pre- and post-reconstructed samples.

The constraint on α, which represents the deviation from the fiducial cosmology (Methods), is $1.050^{+0.030}_{-0.028}$ and $1.057^{+0.035}_{-0.036}$ using the pre- and post-reconstructed samples, respectively. Both results are in good agreement (within 2σ) with the fiducial Planck18 (ref. 22) results (TT, TE, EE + lowE + lensing + BAO), which assumes a Λ cold dark matter model (where Λ is the cosmological constant) cosmology. We find that the constraint is not improved after reconstruction for the GI correlations, which may be due to the fact that we only reconstruct the density field and keep the shape field unchanged. The result may be further improved in principle if the shape field is also reconstructed, which is left for a future study.

The post-reconstructed GG (panel c) and combined (panel d) measurements and modelling are also shown in Fig. 1. The GG correlation alone measures α to be $0.986^{+0.013}_{-0.013}$ and the combined GG + GI derives the constraint to be $0.997^{+0.012}_{-0.012}$, demonstrating that the GI measurement gives rise to a ~10% improvement in terms of the uncertainty on α. More importantly, as we mentioned above, the next-generation surveys can tighten the GG BAO constraints by a factor of 2–3 (refs. 1,23), and systematic errors will become more and more important. If the GI measurements can be improved to the same level, comparisons between sub-per-cent (<0.5%) GG measurements and 1% GI measurements can provide a check of the systematic bias in the measurements. Our GG results are consistent with the results reported by the Baryon Oscillation Spectroscopic Survey (BOSS) team[6] within the 68% confidence level uncertainty, although the numbers are slightly different due to a few effects, including fitting ranges, details of radial bins and error estimations.

In Fig. 3, we convert the constraints on α to distance D_V/r_d measured at redshift z = 0.57, with the fiducial values $D_{V,\rm fid}(0.57)$ = 2,056.58 Mpc, $r_{\rm d,fid}$ = 147.21 Mpc and $D_{V,\rm fid}/r_{\rm d,fid}$ = 13.97 for Planck18 (ref. 22). The quantity D_V/r_d is measured to be $14.67^{+0.42}_{-0.40}$, $14.77^{+0.49}_{-0.50}$, $13.77^{+0.18}_{-0.19}$ and $13.91^{+0.17}_{-0.17}$ using the pre-reconstructed GI, post-reconstructed GI, GG and GI + GG, respectively. All these results are consistent with Planck18 within the 2σ level.

In this work, we obtain a 2–3σ measurement of the BAO dip feature in GI correlations, although the constraints on the distance from GI are only around one-third of those from GG, much weaker than predicted by Taruya and Okumura[21] using the LA model. The reason may be that the galaxy–halo misalignment[24] can reduce the IA signals and weaken the BAO constraints, which may not be considered appropriately by Taruya and Okumura[21]. According to Okumura and Jing[24], on taking into account the misalignment the GI signals can be reduced by two- to

threefold, which is consistent with our results. Moreover, since realistic mock catalogues for galaxy shapes are unavailable as yet, the covariance matrices in this study are estimated using the jackknife resampling method. Employing more reliable error estimation techniques could potentially improve the accuracy of the results, and is left for a future study. Nevertheless, the results are already promising. With the next-generation spectroscopic and photometric surveys including the Dark Energy Spectroscopic Instrument (DESI)[23] and the Legacy Survey of Space and Time[25], we will have larger galaxy samples and better shape measurements. We expect that the IA statistics can provide much tighter constraints on cosmology from BAO and other probes[26,27].

Methods

Statistics of the IA

The shape of galaxies can be characterized by a two-component ellipticity, which is defined as follows:

$$\gamma_{(+,\times)} = \frac{1-q^2}{1+q^2}(\cos(2\theta), \sin(2\theta)) \ , \tag{1}$$

where q represents the minor-to-major axial ratio of the projected shape, and θ denotes the angle between the major axis projected onto the celestial sphere and the projected separation vector pointing towards a specific object.

The GI correlations, denoted as the cross-correlation functions between density and ellipticity fields, can be expressed as[15,18]

$$\xi_{gi}(\mathbf{r}) = \langle [1+\delta_g(\mathbf{x}_1)][1+\delta_g(\mathbf{x}_2)]\gamma_i(\mathbf{x}_2)\rangle. \tag{2}$$

Here, δ_g is the overdensity of galaxies, $\mathbf{r} = \mathbf{x}_1 - \mathbf{x}_2$ and $i = \{+, \times\}$.

In this work, we focus on the GI correlation ξ_{g+} since the signal of $\xi_{g\times}$ vanishes due to parity considerations. It is worth noting that the IA statistics exhibit anisotropy even in real space due to the utilization of projected shapes of galaxies, and the presence of redshift space distortion[28] can introduce additional anisotropies in $\xi_{g+}(\mathbf{r})$. Therefore, we define the multipole moments of the correlation functions as[29]

$$X_\ell(r) = \frac{2\ell+1}{2}\int_{-1}^{1} \mathrm{d}\mu\, X(\mathbf{r})\mathcal{P}_\ell(\mu). \tag{3}$$

Here, X represents one of the correlation functions, $\mathcal{P}_\ell$ denotes the Legendre polynomials and μ corresponds to the directional cosine between $\mathbf{r}$ and the line-of-sight direction.

The LA model

On large scales, the LA model is frequently employed in studies of IAs[14,15,18]. This model assumes a linear relationship between the ellipticity fields of galaxies and halos and the gravitational tidal field.

$$\gamma_{(+,\times)}(\mathbf{x}) = -\frac{C_1}{4\pi G}\left(\nabla_x^2 - \nabla_y^2, 2\nabla_x\nabla_y\right)\Psi_p(\mathbf{x}), \tag{4}$$

where Ψ_p represents the gravitational potential, G denotes the gravitational constant and C_1 characterizes the strength of IA. Although the observed ellipticity field is density weighted, namely $[1+\delta_g(\mathbf{x})]\gamma_{(+,\times)}(\mathbf{x})$, the term $\delta_g(\mathbf{x})\gamma_{(+,\times)}(\mathbf{x})$ is subdominant on large scales[18] because $\delta_g(\mathbf{x}) \ll 1$, and it can be neglected at the BAO scale. In the Fourier space, equation (4) can be expressed as

$$\gamma_{(+,\times)}(\mathbf{k}) = -\widetilde{C}_1\frac{\left(k_x^2 - k_y^2, 2k_xk_y\right)}{k^2}\delta(\mathbf{k}). \tag{5}$$

Here, $\widetilde{C}_1(a) \equiv a^2C_1\bar{\rho}(a)/\bar{D}(a)$, where $\bar{\rho}$ represents the mean mass density of the Universe, $\bar{D}(a) \propto D(a)/a$, and $D(a)$ corresponds to the linear growth factor, with a denoting the scale factor.

Then, $\xi_{g+}(\mathbf{r})$ can be represented by the matter power spectrum $P_{\delta\delta}$[18,30]:

$$\xi_{g+}(\mathbf{r}) = \widetilde{C}_1 b_g(1-\mu^2)\int_0^\infty \frac{k^2\,\mathrm{d}k}{2\pi^2}P_{\delta\delta}(k)j_2(kr), \tag{6}$$

where b_g is the linear galaxy bias and j_2 is the second-order spherical Bessel function.

The redshift space distortion effect[28] can also be considered in $\xi_{g+}(\mathbf{r})$ at large scales[18]. However, in this work, we do not consider the redshift space distortion effect and only focus on the monopole component of $\xi_{g+}(\mathbf{r})$ given the sensitivity of current data.

$$\xi_{g+,0}(r) = \frac{2}{3}\widetilde{C}_1 b_g\int_0^\infty \frac{k^2\,\mathrm{d}k}{2\pi^2}P_{\delta\delta}(k)j_2(kr). \tag{7}$$

We plan to measure the entire two-dimensional $\xi_{g+}(\mathbf{r})$ with future large galaxy surveys, which may contain much more information. To test the LA model, Okumura et al.[20] measured the IA statistics in N-body simulations and found that the results agree well with the predictions from the LA model on large scales. Thus, it is reasonable to use the above formula of $\xi_{g+,0}(r)$ for BAO studies.

Fitting the BAO scale

We fit the BAO features in GG correlations following the SDSS-III BOSS DR12 analysis[6,31].

To model the BAO features in GI correlations, we adopt a methodology similar to that used in GG studies[5,32]. In spherically averaged two-point measurements, the BAO position is fixed by the sound horizon at the baryon-drag epoch r_d and provides a measurement of[4]

$$D_V(z) \equiv \left[cz(1+z)^2D_A(z)^2H^{-1}(z)\right]^{1/3}, \tag{8}$$

where $D_A(z)$ is the angular diameter distance and $H(z)$ is the Hubble parameter. The correlation functions are measured under an assumed fiducial cosmological model to convert angles and redshifts into distances. The deviation of the fiducial cosmology from the true one can be measured by comparing the BAO scale in clustering measurements with its position in a template constructed using the fiducial cosmology. The deviation is characterized by

$$\alpha \equiv \frac{D_V(z)r_{d,fid}}{D_{V,fid}(z)r_d}, \tag{9}$$

where the subscripts 'fid' denote the quantities from the fiducial cosmology.

The template of $\xi_{g+,0}$ is generated using the linear power spectrum, P_{lin}, from the CLASS code[33]. In GG BAO peak fitting, a linear power spectrum with damped BAO is usually used to account for the nonlinear effect,

$$P_{damp}(k) = P_{nw}(k)\left[1+\left(\frac{P_{lin}(k)}{P_{nw}(k)}-1\right)e^{-(1/2)k^2\Sigma_{nl}^2}\right], \tag{10}$$

where P_{nw} is the fitting formula of the no-wiggle power spectrum[3] and Σ_{nl} is the damping scale. In this analysis, we set $\Sigma_{nl} = 0$ as our fiducial model for GI, and we also show the results with Σ_{nl} as a free parameter in Supplementary Table 1.

Using the template, our model for GI correlation is given by

$$\xi_{g+,0}(s) = B\int_0^\infty \frac{k^2\,\mathrm{d}k}{2\pi^2}P_{lin}(k)j_2(\alpha ks), \tag{11}$$

where s is the comoving distance in redshift space and B accounts for all the factors that only affect the amplitude of the correlation, such

as IA strength, galaxy bias and shape responsivity (see equation (16)). As in the GG analysis, we add a further polynomial in our model to marginalize over the broad band shape:

$$\xi^{\rm mod}_{\rm g+,0}(s) = \xi_{\rm g+,0}(s) + \frac{a_1}{s^2} + \frac{a_2}{s} + a_3. \quad (12)$$

Thus, with the observed GI correlation $\xi_{\rm g+,0}{}^{\rm obs}(s)$ and the covariance matrix C, we can assume a likelihood function $\mathcal{L} \propto \exp(-\chi^2/2)$, with

$$\chi^2 = \frac{N_{\rm JK} - N_{\rm bin} - 2}{N_{\rm JK} - 1} \sum_{i,j} [\xi_i{}^{\rm mod} - \xi_i{}^{\rm obs}]\, C^{-1}_{ij}\, [\xi_j{}^{\rm mod} - \xi_j{}^{\rm obs}], \quad (13)$$

where C^{-1} is the inverse of C, i,j indicate the data points at different radial bins, $N_{\rm JK}$ and $N_{\rm bin}$ are the total numbers of subsamples and radial bins and $(N_{\rm JK} - N_{\rm bin} - 2)/(N_{\rm JK} - 1)$ is the Hartlap correction factor[34] to obtain the unbiased covariance matrix. The covariance matrices are estimated using the jackknife resampling from the observation data:

$$C_{ij} = \frac{N_{\rm JK} - 1}{N_{\rm JK}} \sum_{n=1}^{N_{\rm JK}} \left(\xi_i^n - \bar{\xi}_i\right)\left(\xi_j^n - \bar{\xi}_j\right), \quad (14)$$

where ξ_i^n is the measurement in the nth subsample at the ith radial bin and $\bar{\xi}_i$ is the mean jackknife correlation function at the ith radial bin. We use the Markov chain Monte Carlo sampler emcee[35] to perform a maximum-likelihood analysis. $N_{\rm JK}$ is chosen by gradually increasing it until the constraints on α are stable (Supplementary Table 1).

Sample selection

We use the data from the BOSS CMASS DR12 sample[6,36,37]. The CMASS sample covers an effective area of 9,329°^{2} and provides spectra for over 0.8 million galaxies. Galaxies are selected with a number of magnitude and colour cuts to obtain an approximately constant stellar mass. We use the CMASSLOWZTOT Large-Scale Structure catalogue in BOSS DR12 and adopt a redshift cut of $0.43 < z < 0.70$ to select the CMASS sample with an effective redshift $z_{\rm eff} = 0.57$.

Reconstruction methods can improve the significance of the detection of the BAO feature, and reduce the uncertainty in BAO scale measurements, by correcting for the density field smoothing effect associated with large-scale bulk flows[38–40]. We also use the post-reconstructed catalogues from BOSS DR12 and we refer for the details of the reconstruction methods to their papers[6,40].

To obtain high-quality images for the CMASS galaxies, we cross-match them with the DESI Legacy Imaging Surveys DR9 data[41] (https://www.legacysurvey.org/dr9/files/#survey-dr9-region-specobj-dr16-fits), which cover the full CMASS footprint and contain all the CMASS sources. The Legacy Surveys can reach an r-band point spread function depth fainter than 23.5 mag, which is two to three magnitudes deeper than the SDSS photometry survey used for target selection and is more than adequate to study the orientations of the massive CMASS galaxies. The Legacy Survey images are processed using Tractor[42], a forward-modelling approach to perform source extraction on pixel-level data. We use shape_e1 and shape_e2 in the Legacy Surveys DR9 catalogues (https://www.legacysurvey.org/dr9/catalogs/#ellipticities) as the shape measurements for each CMASS galaxy. These two quantities are then converted to the ellipticity defined in equation (1). Following Okumura & Jing[24], we assume that all the galaxies have $q = 0$, which is equivalent to assuming that a galaxy is a line along its major axis. This assumption only affects the amplitude of the GI correlations, and the measurements of the position angles are more accurate than those of the whole galaxy shapes.

The whole CMASS sample is used to trace the density field, while for the tracers of the ellipticity field we further select galaxies with Sérsic index[43] $n > 2$, since only elliptical galaxies show strong shape alignments, and $q < 0.8$ for reliable position angle measurements. In principle, we should also exclude satellite galaxies. However, since selecting centrals in redshift space is arbitrary and most of the CMASS luminous red galaxies are already centrals, we do not consider the central–satellite separation. Selections using n and q remove nearly half (from 816,779 to 425,823) of the CMASS galaxies. We show the results using the whole sample in Supplementary Table 1 and confirm that the morphology and q selection can really improve the measurements and tighten the constraints.

Estimators

To estimate the GI correlations, we generate two random samples R_s and R for the tracers of ellipticity and density fields respectively. Following Reid et al.[37], redshifts are assigned to randoms to make sure that the galaxy and random catalogues have exactly the same redshift distribution. We adopt the generalized Landy–Szalay estimator[44,45]

$$\xi_{\rm g+,0}(s) = \frac{S_+(D - R)}{R_s R}, \quad (15)$$

where R_sR is the normalized random–random pairs. S_+D is the sum of the + component of ellipticity in all pairs:

$$S_+D = \sum_{i,j} \frac{\gamma_+(j|i)}{2\mathcal{R}}, \quad (16)$$

where the ellipticity of the jth galaxy in the ellipticity tracers is defined relative to the direction to the ith galaxy in the density tracers, and $\mathcal{R} = 1 - \langle\gamma_+^2\rangle$ is the shape responsivity[46]. $\mathcal{R} = 0.5$ under our $q = 0$ assumption. S_+R is calculated in a similar way using the random catalogue.

We also measure the GI correlation functions for the reconstructed catalogues. The ellipticities of galaxies are assumed unchanged in the reconstruction process. The estimator becomes

$$\xi_{\rm g+,0}(s) = \frac{S_+(E - T)}{R_s R}, \quad (17)$$

where E and T represent the reconstructed data and random sample, and R and R_s are the original random samples. In the above calculations, we adopt the Feldman–Kaiser–Peacock weights[47] ($w_{\rm FKP}$) and weights for correcting the redshift failure ($w_{\rm zf}$), fibre collisions ($w_{\rm cp}$) and image systematics ($w_{\rm sys}$) for the density field tracers[37]: $w_{\rm tot} = w_{\rm FKP} w_{\rm sys}(w_{\rm cp} + w_{\rm zf} - 1)$, while no weight is used for the ellipticity field tracers.

Measurements and modelling

We measure $\xi_{\rm g+,0}(s)$ for both pre- and post-reconstruction catalogues in $50 < s < 200\ h^{-1}$ Mpc with a bin width of $5\ h^{-1}$ Mpc. We calculate their covariance matrices using the jackknife resampling with $N_{\rm JK} = 400$, and model the GI correlation functions using equation (11) with a Planck18 (ref. 22) fiducial cosmology at $z = 0.57$. In Supplementary Table 1, we show that the pre- and post-reconstruction GI results are relatively stable if $N_{\rm JK} \geq 400$, verifying that $N_{\rm JK} = 400$ is a reasonable choice. We measure and model the post-reconstruction isotropic GG correlation functions with the same radial bins and error estimation schedule ($N_{\rm JK} = 400$). We also model the GG and GI correlation together with a 60×60 covariance matrix that includes the GG–GI cross-covariance to obtain the combined results.

Data availability

All data used in this study are publicly available. SDSS-III BOSS DR12 Large-Scale Structure catalogue: https://data.sdss.org/sas/dr12/boss/lss/. DESI Legacy Imaging Surveys DR9 catalogue: https://www.legacysurvey.org/dr9/catalogs/.

References

1. Weinberg, D. H. et al. Observational probes of cosmic acceleration. *Phys. Rep.* **530**, 87–255 (2013).

2. Peebles, P. J. E. & Yu, J. T. Primeval adiabatic perturbation in an expanding Universe. *Astrophys. J.* **162**, 815–836 (1970).
3. Eisenstein, D. J. & Hu, W. Baryonic features in the matter transfer function. *Astrophys. J.* **496**, 605–614 (1998).
4. Eisenstein, D. J. et al. Detection of the baryon acoustic peak in the large-scale correlation function of SDSS luminous red galaxies. *Astrophys. J.* **633**, 560–574 (2005).
5. Percival, W. J. et al. Baryon acoustic oscillations in the Sloan Digital Sky Survey Data Release 7 galaxy sample. *Mon. Not. R. Astron. Soc.* **401**, 2148–2168 (2010).
6. Alam, S. et al. The clustering of galaxies in the completed SDSS-III Baryon Oscillation Spectroscopic Survey: cosmological analysis of the DR12 galaxy sample. *Mon. Not. R. Astron. Soc.* **470**, 2617–2652 (2017).
7. Ata, M. et al. The clustering of the SDSS-IV extended Baryon Oscillation Spectroscopic Survey DR14 quasar sample: first measurement of baryon acoustic oscillations between redshift 0.8 and 2.2. *Mon. Not. R. Astron. Soc.* **473**, 4773–4794 (2018).
8. du Mas des Bourboux, H. et al. The completed SDSS-IV Extended Baryon Oscillation Spectroscopic Survey: baryon acoustic oscillations with Lyα forests. *Astrophys. J.* **901**, 153 (2020).
9. Heavens, A., Refregier, A. & Heymans, C. Intrinsic correlation of galaxy shapes: implications for weak lensing measurements. *Mon. Not. R. Astron. Soc.* **319**, 649–656 (2000).
10. Croft, R. A. C. & Metzler, C. A. Weak-lensing surveys and the intrinsic correlation of galaxy ellipticities. *Astrophys. J.* **545**, 561–571 (2000).
11. Hirata, C. M. et al. Intrinsic galaxy alignments from the 2SLAQ and SDSS surveys: luminosity and redshift scalings and implications for weak lensing surveys. *Mon. Not. R. Astron. Soc.* **381**, 1197–1218 (2007).
12. Okumura, T., Jing, Y. P. & Li, C. Intrinsic ellipticity correlation of SDSS luminous red galaxies and misalignment with their host dark matter halos. *Astrophys. J.* **694**, 214–221 (2009).
13. Xu, K., Jing, Y. P. & Gao, H. Mass dependence of galaxy-halo alignment in LOWZ and CMASS. Preprint at *arXiv* https://doi.org/10.48550/arXiv.2302.04230 (2023).
14. Crittenden, R. G., Natarajan, P., Pen, U.-L. & Theuns, T. Spin-induced galaxy alignments and their implications for weak-lensing measurements. *Astrophys. J.* **559**, 552–571 (2001).
15. Hirata, C. M. & Seljak, U. Intrinsic alignment–lensing interference as a contaminant of cosmic shear. *Phys. Rev. D* **70**, 063526 (2004).
16. Blazek, J., McQuinn, M. & Seljak, U. Testing the tidal alignment model of galaxy intrinsic alignment. *J. Cosmol. Astropart. Phys.* **2011**, 010 (2011).
17. Chisari, N. E. & Dvorkin, C. Cosmological information in the intrinsic alignments of luminous red galaxies. *J. Cosmol. Astropart. Phys.* https://doi.org/10.1088/1475-7516/2013/12/029 (2013).
18. Okumura, T. & Taruya, A. Anisotropies of galaxy ellipticity correlations in real and redshift space: angular dependence in linear tidal alignment model. *Mon. Not. R. Astron. Soc.* **493**, L124–L128 (2020).
19. van Dompseler, D., Georgiou, C. & Chisari, N. E. The alignment of galaxies at the Baryon Acoustic Oscillation scale. Preprint at *arXiv* https://doi.org/10.48550/arXiv.2301.04649 (2023).
20. Okumura, T., Taruya, A. & Nishimichi, T. Testing tidal alignment models for anisotropic correlations of halo ellipticities with *N*-body simulations. *Mon. Not. R. Astron. Soc.* **494**, 694–702 (2020).
21. Taruya, A. & Okumura, T. Improving geometric and dynamical constraints on cosmology with intrinsic alignments of galaxies. *Astrophys. J. Lett.* **891**, L42 (2020).
22. Planck Collaborationet al. Planck 2018 results. VI. Cosmological parameters. *Astron. Astrophys.* **641**, A6 (2020).
23. DESI Collaboration et al. The DESI Experiment part I: science, targeting, and survey design. Preprint at *arXiv* https://doi.org/10.48550/arXiv.1611.00036 (2016).
24. Okumura, T. & Jing, Y. P. The gravitational shear–intrinsic ellipticity correlation functions of luminous red galaxies in observation and in the ΛCDM model. *Astrophys. J. Lett.* **694**, L83–L86 (2009).
25. Ivezić, Ž. et al. LSST: from science drivers to reference design and anticipated data products. *Astrophys. J.* **873**, 111 (2019).
26. Okumura, T. & Taruya, A. First constraints on growth rate from redshift-space ellipticity correlations of SDSS galaxies at $0.16 < z < 0.70$. *Astrophys. J. Lett.* **945**, L30-L36 (2023).
27. Kurita, T. & Takada, M. Constraints on anisotropic primordial non-Gaussianity from intrinsic alignments of SDSS-III BOSS galaxies. Preprint at *arXiv* https://doi.org/10.48550/arXiv.2302.02925 (2023).
28. Kaiser, N. Clustering in real space and in redshift space. *Mon. Not. R. Astron. Soc.* **227**, 1–21 (1987).
29. Hamilton, A. J. S. Measuring omega and the real correlation function from the redshift correlation function. *Astrophys. J. Lett.* **385**, L5 (1992).
30. Okumura, T., Taruya, A. & Nishimichi, T. Intrinsic alignment statistics of density and velocity fields at large scales: formulation, modeling, and baryon acoustic oscillation features. *Phys. Rev. D* **100**, 103507 (2019).
31. Wang, Y. et al. The clustering of galaxies in the completed SDSS-III Baryon Oscillation Spectroscopic Survey: tomographic BAO analysis of DR12 combined sample in configuration space. *Mon. Not. R. Astron. Soc.* **469**, 3762–3774 (2017).
32. Anderson, L. et al. The clustering of galaxies in the SDSS-III Baryon Oscillation Spectroscopic Survey: baryon acoustic oscillations in the Data Releases 10 and 11 galaxy samples. *Mon. Not. R. Astron. Soc.* **441**, 24–62 (2014).
33. Lesgourgues, J. The Cosmic Linear Anisotropy Solving System (CLASS) I: overview. Preprint at *arXiv* https://doi.org/10.48550/arXiv.1104.2932 (2011).
34. Hartlap, J., Simon, P. & Schneider, P. Why your model parameter confidences might be too optimistic. Unbiased estimation of the inverse covariance matrix. *Astron. Astrophys.* **464**, 399–404 (2007).
35. Foreman-Mackey, D., Hogg, D. W., Lang, D. & Goodman, J. emcee: the MCMC hammer. *Publ. Astron. Soc. Pac.* **125**, 306–312 (2013).
36. Alam, S. et al. The Eleventh and Twelfth Data Releases of the Sloan Digital Sky Survey: final data from SDSS-III. *Astrophys. J. Suppl.* **219**, 12 (2015).
37. Reid, B. et al. SDSS-III Baryon Oscillation Spectroscopic Survey Data Release 12: galaxy target selection and large-scale structure catalogues. *Mon. Not. R. Astron. Soc.* **455**, 1553–1573 (2016).
38. Eisenstein, D. J., Seo, H.-J., Sirko, E. & Spergel, D. N. Improving cosmological distance measurements by reconstruction of the baryon acoustic peak. *Astrophys. J.* **664**, 675–679 (2007).
39. Padmanabhan, N., White, M. & Cohn, J. D. Reconstructing baryon oscillations: a Lagrangian theory perspective. *Phys. Rev. D* **79**, 063523 (2009).
40. Padmanabhan, N. et al. A 2 per cent distance to $z=0.35$ by reconstructing baryon acoustic oscillations—I. Methods and application to the Sloan Digital Sky Survey. *Mon. Not. R. Astron. Soc.* **427**, 2132–2145 (2012).
41. Dey, A. et al. Overview of the DESI Legacy Imaging Surveys. *Astron. J.* **157**, 168 (2019).
42. Lang, D., Hogg, D. W. & Mykytyn, D. The Tractor: probabilistic astronomical source detection and measurement. *Astrophysics Source Code Library* ascl:1604.008 (2016).

43. Sérsic, J. L. Influence of the atmospheric and instrumental dispersion on the brightness distribution in a galaxy. *Bol. Asoc. Argent. Astron.* **6**, 41–43 (1963).
44. Landy, S. D. & Szalay, A. S. Bias and variance of angular correlation functions. *Astrophys. J.* **412**, 64–71 (1993).
45. Mandelbaum, R., Hirata, C. M., Ishak, M., Seljak, U. & Brinkmann, J. Detection of large-scale intrinsic ellipticity–density correlation from the Sloan Digital Sky Survey and implications for weak lensing surveys. *Mon. Not. R. Astron. Soc.* **367**, 611–626 (2006).
46. Bernstein, G. M. & Jarvis, M. Shapes and shears, stars and smears: optimal measurements for weak lensing. *Astron. J.* **123**, 583–618 (2002).
47. Feldman, H. A., Kaiser, N. & Peacock, J. A. Power-spectrum analysis of three-dimensional redshift surveys. *Astrophys. J.* **426**, 23 (1994).

Acknowledgements

Y.P.J. is supported by NSFC (12133006, 11890691, 11621303), grant CMS-CSST-2021-A03, and 111 project B20019. Y.P.J. gratefully acknowledges the support of the Key Laboratory for Particle Physics, Astrophysics and Cosmology, Ministry of Education. G.-B.Z. is supported by the National Key Basic Research and Development Program of China (2018YFA0404503), NSFC (11925303, 11890691), science research grants from the China Manned Space Project (CMS-CSST-2021-B01) and the New Cornerstone Science Foundation through the XPLORER PRIZE. A.J.C. acknowledges support from the Spanish Ministry of Science, Innovation and Universities (PID2019-107844GB-C21/AEI/10.13039/501100011033), and funding from the European Union—Next Generation EU and the Ministerio de Universidades of Spain through Plan de Recuperación, Transformación y Resiliencia. This work made use of the Gravity Supercomputer at the Department of Astronomy, Shanghai Jiao Tong University. K.X. thanks J. Zhang for helpful discussions.
Funding for SDSS-III has been provided by the Alfred P. Sloan Foundation, the Participating Institutions, the National Science Foundation and the US Department of Energy Office of Science. The SDSS-III web site is http://www.sdss3.org/.
The Legacy Surveys consist of three individual and complementary projects: the Dark Energy Camera Legacy Survey (DECaLS; proposal 2014B-0404; principal investigators D. Schlegel and A. Dey), the Beijing–Arizona Sky Survey (BASS; NOAO proposal 2015A-0801; principal investigators Z. Xu and X. Fan) and the Mayall z-band Legacy Survey (MzLS; proposal 2016A-0453; principal investigator A. Dey).

Author contributions

Y.P.J. proposed the idea and supervised the work. K.X. performed the measurements and modelling. A.J.C. provided tools and expertise with the public data catalogues. K.X. and G.-B.Z. wrote the draft. All co-authors contributed to the improvement of the analysis and the manuscript.

Competing interests

The authors declare that they have no competing interests.

Additional information

Supplementary information The online version contains supplementary material available at https://doi.org/10.1038/s41550-023-02035-4.

Correspondence and requests for materials should be addressed to Y. P. Jing.

Peer review information *Nature Astronomy* thanks Mariana Vargas Magana and the other, anonymous, reviewer(s) for their contribution to the peer review of this work.